Journal of Materials Chemistry

Dynamic Article Links

Cite this: J. Mater. Chem., 2012, 22, 5398

www.rsc.org/materials

PAPER

Size and shape matter! A multiscale molecular simulation approach to polymer nanocomposites†‡

Radovan Toth,[a] Francesca Santese,[a] Simão P. Pereira,[ab] Daniel R. Nieto,[a] Sabrina Pricl,[a] Maurizio Fermeglia[a] and Paola Posocco*[a]

Received 9th November 2011, Accepted 5th January 2012
DOI: 10.1039/c2jm15763b

Multiscale molecular modelling (MsM) techniques are applied in many fields of material science, but it is particularly important in the polymer field, due to the wide range of phenomena occurring at different scales which influence the ultimate properties of the materials. In this context, MsM plays a crucial role in the design of new materials whose properties are influenced by the structure at the nanoscale. In this work we present the application of a multiscale molecular modelling procedure to characterize a different set of polymer-based nanocomposites (PNCs) obtained with full/partial dispersion of different nanofillers in different polymeric matrices. This approach relies on a step-by step message-passing technique from atomistic to mesoscale to finite element level, and the calculated results are compared to available experimental evidence. In detail, 13 PNC systems have been studied by different molecular modelling methods, such as atomistic molecular mechanics and molecular dynamics, mesoscale dissipative particles dynamics, and macroscale finite element methods, and their mechanical, thermal and barrier properties have been predicted in agreement with the available experimental data.

1 Introduction

Manufacturers and producers add nanoparticles to polymers in order to improve the stiffness and the toughness of the materials, to amend their barrier properties, to enhance their resistance to fire and ignition or, simply, to reduce costs. These nanofillers come in the form of different shapes, such as spheres,[1] tubes,[2] platelets and discs,[3–5] or fibres.[6,7] The fact that both scientific and industrial interest in this new class of materials, generally termed polymer nanocomposites (PNCs), have skyrocketed in the last few decades is not in question.[8–10] However, the production of these nanomaterials still includes various accustomed techniques, their preparation is still largely empirical, and a finer degree of control of their ultimate properties cannot be achieved so far. Thus, from an experimental point of view, at least two grand challenges remain: (i) the structural characterization and (ii) the precise manipulation of the fabrication of these hybrid nanostructure materials. As the final properties of PNCs commonly depend on their structure, a detailed knowledge of the morphology of each PNC system is of paramount importance. To this purpose, the development of theories and the application of computer simulation techniques have opened avenues for the design of these materials, and the *a priori* prediction/optimization of their structures and properties.[11]

A nanocomposite is a material in which at least one of its components has dimensions within the nanometre level.[12] This definition is grounded on well-established principles that govern material behaviour, as documented by Feynman over half a century ago.[13] In his lecture he stated: "Atoms on a small scale behave like nothing on a large scale, for they satisfy the laws of quantum mechanics. So, as we go down and fiddle around with the atoms down there, we are working with different laws and we can expect different things". In other words, as the size scale of matter becomes smaller, down to the nanoscale, the material behaviour can be understood on the basis of intermolecular forces (*e.g.*, van der Waals and hydrogen bonding, electrostatic attractions and repulsions, or steric repulsions). Since all of these forces have a limited distance of influence, ranging from a few angstroms to a few nanometres, proper tools and techniques need to be involved in the characterization process in order to provide detailed information about behaviour, structural morphology, and final properties of such nanomaterials. A multiscale molecular modelling approach which bridges the macroscale properties of matter to its atomistic nature *via* its

[a]*MOSE-Lab, DI3, University of Trieste, Via Valerio 10, 34127 Trieste, Italy. E-mail: paola.posocco@di3.units.it; Fax: +39 040 569823; Tel: +39 040 5583440*
[b]*IPC/I3N-Institute for Polymers and Composites, Department of Polymer Engineering, University of Minho, Campus de Azurém, Guimarães, 4800-058, Portugal*

† This work is dedicated to the fond memory of Dr Daniela Tabuani, colleague and friend, unexpectedly and prematurely deceased on October 28, 2011.

‡ Electronic supplementary information (ESI) available: Full version of the computational details. See DOI: 10.1039/c2jm15763b

mesoscopic morphology can be one of those techniques, as its field of operation covers levels ranging from angstroms to micrometres.

Multiscale molecular modelling (MsM) of polymer-based nanocomposite materials poses formidable challenges due to the huge range of length and time scales involved, influencing their structures and physical properties.[14] These challenges can only be met through the development of suitable hierarchical analysis and simulation strategies encompassing many interconnected levels, where each level addresses a phenomenon over a specific window of length and time. Several computational approaches—spanning different length/time scale domains—have been proposed in recent years for the characterization of PNCs, including molecular mechanics (MM) and molecular dynamics (MD),[15] mesoscale (MS),[16] and finite element simulations (FEM).[17] MsM was shown to be a valuable tool for characterization and/or prediction of macroscopic properties of polymer nanocomposites with different fillers, as layered clays,[18] carbon nanotubes,[19–21] boron nanotubes,[22] fibres,[23,24] or spheres.[25]

In our previous works[26] we developed MsM tools that model polymer-based nanocomposite systems from the molecular to the continuum scale. Although each tool performs independent calculations by using only one method at a time, the output from one method can be used directly as the input for another, allowing an off-line bridging between the different scales. Further, our recent efforts in the field of molecular modelling also consisted of atomistic calculations concerned with binding energy evaluations for well-characterized systems[26a–d] using molecular mechanics and molecular dynamics (MM/MD) methods. At the same time, part of our activities was focused on the development and application of mesoscale simulation (MS) tools to polymer blends and nanocomposites morphology investigations, and on the integration of these tools with both atomistic[26e–h,m,n] and macroscale approaches through finite element method calculations.[26i,j,l]

Based on this experience, in this paper we used our wealth of knowledge for a thorough characterization of a set of different PNCs of industrial interest. In detail, we studied the behaviour of different nanofillers (pristine or modified by the addition of, *e.g.*, a compatibilizer) in different polymer matrices (see Table 1) by using a multiscale molecular modelling protocol. This has the final aim of (i) predicting some fundamental macroscopic properties of existing nanocomposite materials, (ii) comparing them with the available experimental data, and (iii) ascertaining the robustness and validity of this *in silico* approach as a valuable, less-expensive, and time-saving tool for the design of new PNCs with desired performances.

The paper is organized as follows: first, the binding energy values among all system components obtained from MD atomistic simulations for all PCNs are reported and commented. Then, the PNC morphologies predicted at the mesoscopic level are presented and discussed. Finally, a set of macroscopic properties estimated *via* FEM calculations are given and major conclusions are drawn.

Table 1 Names and compositions of polymer-based nanostructured systems studied in this work. Abbreviations: PP = poly(propylene); PA6 = poly(amide) 6; TPU = thermoplastic poly(urethane); MMT = montmorillonite (platelets); HT = hydrotalcite (platelets); SEP = sepiolite (fibres); BOE = boehmite (spheres); TiO_2 = titania (spheres)

System	Matrix	Filler	Surface modifier
PP/C10A[a]	PP	MMT	$(H_3C)_2N(C_{18}H_{37})(C_2H_4Ph)$
PP/C15A[a]	PP	MMT	$(H_3C)_2N(C_{18}H_{37})_2$[f]
PP/C20A[a]	PP	MMT	$(H_3C)_2N(C_{18}H_{37})_2$[f]
PP/C30B[a]	PP	MMT	$(H_3C)N(C_{18}H_{37})(C_2H_4OH)_2$
PP/ODA	PP	MMT	$H_3N(C_{18}H_{37})$
PA6/C20A[a]	PA6	MMT	$(H_3C)_2N(C_{18}H_{37})_2$
PA6/C30B[a]	PA6	MMT	$(H_3C)N(C_{18}H_{37})(C_2H_4OH)_2$
PA6/M_3C_{18}	PA6	MMT	$(H_3C)_3N(C_{18}H_{37})$
TPU[b]/C30B	TPU	MMT	$(H_3C)N(C_{18}H_{37})(C_2H_4OH)_2$
PP/HT[c]/FA	PP	HT	C_{16}–C_{18} fatty acids
PP/SEP[d]	PP	SEP	No surfactant
PP/BOE[e]	PP	BOE	No surfactant
PP/TiO_2	PP	TiO_2	No surfactant

[a] Cloisites C10A, C15A, C20A, and C30B, Southern Clay, USA. [b] Elastollan 1185A, BASF, Germany. [c] F100, Akzo Nobel, The Netherlands. [d] CD1, Tolsa, Spain. [e] Disperal, Sasol, Germany. [f] Cloisites C15A and C20A have the same surface modifier but differ in cation exchange capacity (CEC): 125 and 95 mequiv. per 100 g clay, respectively.

2 Simulation procedure and computational details

The proposed computational procedure of the multiscale simulation and modelling (see ESI‡ for full details) is based on the following ansatz: (1) fully atomistic molecular dynamics simulations are performed to retrieve fundamental structural and energetical information at the molecular level; (2) the data gathered at point (1) are mapped into the corresponding structural and energetical information necessary to run coarse-grained simulations at a mesoscopic level; (3) the main output of point (2), *i.e.*, the mesoscopic morphologies and density distributions of the system finally constitute the input for finite element calculations and macroscopic property predictions. The core step in the entire computational recipe is undoubtedly constituted by point (2), or the mesoscale level simulations. In mesoscale modelling, the familiar atomistic description of the molecules is coarse-grained, leading to beads of material (representing the collective degrees of freedom of many atoms). These beads interact through pair-potentials which capture the underlying interactions of the constituent atoms. The primary output of mesoscale modelling is phase morphologies with size up to the micron level. These morphologies are of interest *per se*, although little prediction of the material properties is available with the mesoscale tools. Finite element modelling then comes into play, and the material properties of interest can be calculated accordingly by mapping the material structures formed at the nanometre scale onto the finite element grid and coupling this information with the properties of the pure components that comprise the complex system. Using standard solvers the finite element code can then be applied to calculate the properties of the realistic structured material. Fig. 1 presents the so-called 'multiscale simulation protocol', which can be used as template for calculation of macroscopic property of different nanoscale systems.

2.1 Atomistic molecular dynamics (MD) simulations

As mentioned above, atomistic MD simulations constitute the first MsM step, necessary to gather basic structural and

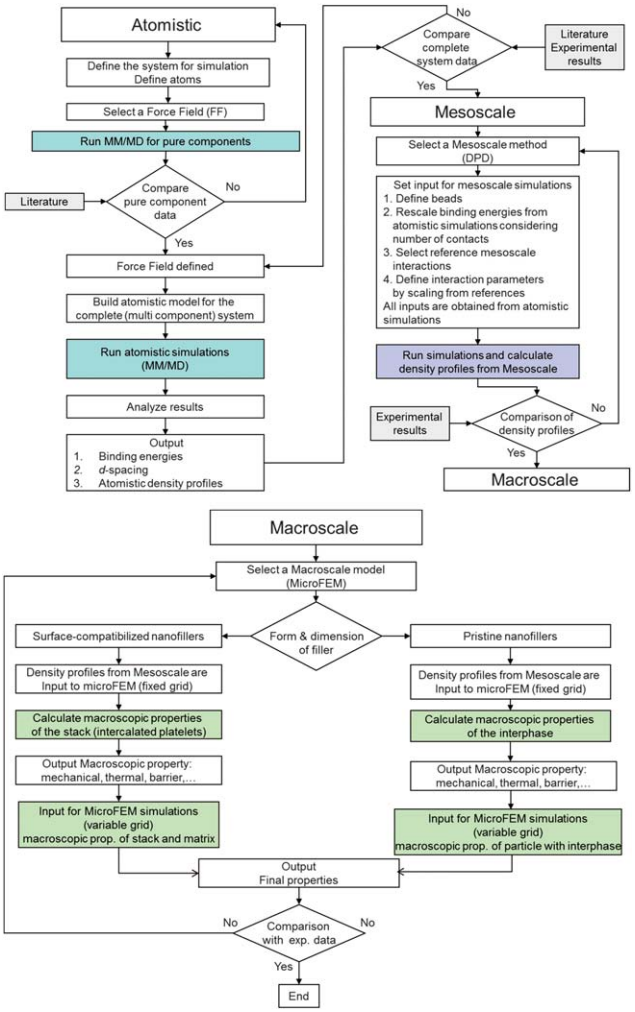

Fig. 1 General scheme of the multiscale simulation protocol for the study of PNCs adopted in this work.

energetical information of each PNC system at the molecular level. In particular, the interaction energies among all system components are of paramount importance, as they will, after proper remapping, constitute the major input parameter for performing mesoscale simulations. Hence, the choice of a reliable force field for the description of inter- and intra-molecular interactions in atomistic MD simulations is a critical issue in the entire protocol. Our previous experience,[26] coupled with a thorough literature survey,[15,27] led us to the adoption of the *Compass* force field (FF).[28,29]

The optimized montmorillonite (MMT) model was taken from our previous work.[26c,k] Starting from the crystal coordinates of Mg/Al hydrotalcite as determined by Bellotto *et al.*,[30] the 3D model of hydrotalcite (HT) was built and optimized by adapting the procedure adopted for MMT.[26c,k] The unit cells of sepiolite (SEP), boehmite (BOE), and titanium dioxide (rutile form, TiO_2) were optimized starting from the original structures available in the *Materials Studio* (v.5.5, Accelrys, USA) structure database. To generate a mineral surface apt for simulation, the lattice constant c of each mineral cell was extended to 150 Å,[26c,d] while the lateral dimensions of the cell were increased to the point where the total number of atoms in each model was approximately equal.

The model structures of the MMT and HT surface modifiers (*i.e.*, quaternary ammonium salts and C16–C18 fatty acids, respectively) were built and subjected to an initial energy minimization process followed by a thorough conformational search.[31] The generation of accurate model amorphous structures for polymers was conducted following a consolidated recipe.[26]

After each component was modelled, the overall PNC systems were built,[26c,d] and production molecular dynamics simulations in the canonical (NVT) ensemble were run at $T = 298$ K. From the equilibrated part of the MD trajectory of each PNC, the interaction energies among all system components were extracted according to a well-validated procedure.[26] Since, by definition, the binding energy (E_{bind}) between each generic pair of PNC components A and B is the negative of the corresponding interaction energy, each E_{bind} term can be simply obtained from the corresponding interaction energies as:[26]

$$E_{bind(A/B)} = E_A + E_B - E_{A/B} \quad (1)$$

In the case of modified nanoparticles (*i.e.*, MMT and HT), starting from an equilibrated NVT MD snapshot further MD simulations in the isothermal–isobaric (NPT) ensemble were performed to estimate the interlayer (basal) spacing d among the mineral layers.[26c,k,i] In this case, during each MD both mineral layers were treated as rigid bodies by fixing all cell dimensions except for c, and all atoms in the interlayer space (including ions and counterions) were allowed to move without any constraint.

2.2 Mesoscale (MS) simulations of PNCs

In order to simulate the morphology of the nanocomposite systems at a mesoscopic level, we used the dissipative particle dynamics (DPD)[32] simulation tool as implemented in the *Materials Studio* DPD modelling suite.

In the framework of our multiscale approach to PNCs simulation, the interaction parameters needed as input for the mesoscale level DPD calculations have been obtained by a mapping procedure of the binding energy values between different species obtained from simulations at a lower (atomistic) scale.[26e,i] The complex procedure for mesoscale simulation of our PNC systems consists of several steps: (i) choice of the bead size, (ii) determination of system dimension and bead numbers, and (iii) definition of bead–bead interaction parameters.[26e,i,l–n] In the case of surface-modified nanocomposites, according to the fundamental DPD concept that different DPD bead types should have roughly equal volumes, and starting with the surface modifier molecules (which consist of a strongly polar head and one/two almost apolar tails) we considered them as made up of two different types of beads, H and T, respectively. The corresponding mesoscopic polymer chains were chosen to be constituted of 100 beads of type P. To represent the filler surface, a repulsive wall in the simulation box perpendicular to the z-axis at the origin was employed. Further, we introduced a bead type M with no connectivity and no repulsion towards the wall, in order to fill the space between the two wall surfaces, thus representing a nanofiller layer.

A parallel approach and utterly similar concepts were used to build all remaining PNCs. In the case of unmodified nanoparticle-based PNCs, however, the corresponding mesoscopic cells contained only two types of beads; indeed, beads of the type M were again used to represent the filler (*i.e.*, SEP, BOE, and TiO_2), and beads of the type P were still employed for the polymers.

The next, important issue in DPD simulations is to capture the essential intra- and inter-molecular interactions taking place among all molecular actors of the mesoscopic simulations as expressed by the values of the conservative parameter a_{ij}. This quantity accounts for the underlying chemistry of the system considered. In this work, we employed a well-validated strategy that correlates the interaction energies estimated from a lower scale (atomistic MD) simulations to the mesoscale a_{ij} parameter values.[33] Following this computational recipe, the interaction energies among all PNC system components estimated from MD simulations were rescaled onto the corresponding mesoscale segments adapting the procedure described in our work.[26e,i] The entire set of DPD interaction parameters employed in this work are summarized in Table 2.

2.3 Finite element (FEM) calculations

The last step of the proposed MsM procedure is constituted by the prediction of a set of important macroscopic properties for the considered polymer nanocomposites as a function of filler loading. For this purpose, finite element (FE) calculations were performed using the software Palmyra (v. 2.5, MatSim, Zürich, CH). This software has been validated on different composite material morphologies by several authors, including us,[26i,k,l,34,35] yielding reliable results. FE calculations were applied in order to analyse both platelet stacks and overall nanocomposite properties, using the fixed (*i.e.*, *MesoProp* technique)[36] and the variable grid methods, respectively. In particular, the Young's modulus E, the thermal conductivity κ, and the gas permeability P were the macroscopic properties of election, since not only these quantities are of primary industrial interest but, perhaps more importantly, direct comparison with the corresponding experimental data could be made.[37]

Following our previous work,[26i,k] MMT and HT particles (both single particles and stacks) were modelled as disks with a toroidal rim. Each platelet thickness was defined by the height of the corresponding symmetry axis h and diameter D, thus being characterized by an aspect ratio of $a = D/h$. By setting $D =$ 120 nm and $h = 1$ nm for each single particle, the aspect ratio a was equal to 120, a value in agreement with common literature data for layer silicates. Orientation to the platelets was imparted by assigning a value of 0.06 to the eigenvalues 1 and 2. Accordingly a value of 0.88 was automatically assigned to the eigenvalue 3. A highly exfoliated system was defined as having 32 platelets with an aspect ratio of 120 and 8 stacks of two platelets each. Such a system corresponds to 66.7% exfoliated platelets. The aspect ratio of the stacks ranged from 10 to 13, according to the different basal spacings obtained from the corresponding MD simulations. To simulate a weight fraction Φ_w of 4.6% w/w for all MMT and HT PNCs, a volume fraction Φ_v of 1.5% v/v was used in the case of PP-based PNCs, while a value of $\Phi_v =$ 1.9% v/v was employed for TPU- and PA6-based systems, respectively. TiO_2 particles were considered as spheres with diameter $\varphi_{TiO2} = 20$ nm. A volume fraction of 1.07% v/v was used, resulting in a corresponding weight fraction of 4.6% w/w. Boehmite is generally synthesized in crystallites of a platelet or rod shape. The widely employed commercial sample Disperal, however, consists of agglomerated small crystallites. During

Table 2 Bead–bead interaction parameter a_{ij} values used in the DPD simulations of all PNC systems considered in this work

a_{ij}	P	T	H	M	W
PP/C10A					
P	25	31	30.9	32	320
T	31	31.3	35.3	30.4	304
H	30.9	35.3	55.5	5.2	52
M	32	30.4	5.2	15	1
PP/C15A					
P	25	29.5	33.6	34	340
T	29.5	32.2	35	30.7	307
H	33.6	35	62.2	3.5	35
M	34	30.7	3.5	15	1
PP/C20A					
P	25	32.7	32.6	33	330
T	32.7	32.8	36	30.7	307
H	32.6	36	64.2	4	50
M	33	30.7	4	15	1
PP/C30B					
P	25	31.1	31	31	310
T	31.1	30.3	32.9	30.1	301
H	31	32.9	54.1	4.7	47
M	31	30.1	4.7	15	1
PP/ODA					
P	25	31	30.9	32	320
T	31	31.3	35.3	30.4	304
H	30.9	35.3	55.5	5.2	52
M	32	30.4	5.2	15	1
PA6/C20A					
P	25	33.6	34.1	33.1	331
T	33.6	32.11	33.1	30.7	307
H	34.1	33.1	62.4	4.1	41
M	33.1	30.7	4.1	15	1
PA6/C30B					
P	25	32	30	29	290
T	32	30.2	32.7	30.1	301
H	30	32.7	54.3	4.7	47
M	29	30.1	4.7	15	1
PA6/M3C18					
P	25	31.5	31.1	31.8	318
T	31.5	31.8	30.9	30.6	306
H	31.1	30.9	55.1	5.2	52
M	31.8	30.6	5.2	15	1
TPU/C30B					
P	25	32.5	33.3	31	310
T	32.5	31.1	35.8	30.8	308
H	33.3	35.8	55.2	4	40
M	31	30.8	4	15	1
PP/HT/FA					
P	25	23.3	28.2	24	240
T	23.3	31	24.5	22	220
H	28.2	24.5	57	3	30
M	24	22	3	15	1
PP/SEP					
P	25	—	—	30.4	304
M	30.4	—	—	15	1
PP/BOE					
P	25	—	—	29	290
M	29	—	—	15	1
PP/TiO_2					
P	25	—	—	30.4	304
M	30.4	—	—	15	1

processing, the agglomerates decrease in size, but still the complete dispersion of the crystallites cannot be achieved.[38] Accordingly, this system was defined considering spherical agglomerates of BOE with an average φ of 140 nm.[39] A volume fraction of 1.43% v/v was used, corresponding to a system with a weight fraction of 4.6% w/w. Finally, the commercial CD1 sepiolite fibres were assumed to have a length $L = 200$ nm and a diameter $\varphi_{SEP} = 10$ nm. A $\Phi_v = 2.1\%$ v/v was considered, corresponding to a system with $\Phi_w = 4.6\%$ w/w.

Interfacial interactions, however, invariably develop in composite systems based on untreated nanofillers, due to the ever-existing van der Waals or electrostatic forces among the particles and the polymer chains. These lead to the formation of a non-negligible interface which, in turn, may considerably influence the macroscopic properties of the relevant PNC. To account for the presence of this interphase layer in the BOE, SEP, and TiO_2 systems, as determined from mesoscale simulations (*vide infra*), we resorted to pseudo-"core–shell" model particles at the FEM level. These models consist of spherical (for BOE and TiO_2) and spherocylindrical (for SEP) particles with radius equal to the sum of the pristine nanoparticle radius (constituting the "core" part of the particle) and the interface thickness (making up the "shell"). Overall, the main thermophysical properties of these particles were then estimated by mediating each corresponding property of the nanoparticle core (*i.e.*, the pure nanoparticle property) and of the interphase (as obtained by running fixed-grid calculations using the mesoscopic density distribution as input information) by the corresponding volumetric fractions.

As mentioned previously, the density profiles of each component obtained from mesoscale simulations were used as an input for macroscopic property calculation of the stacks for intercalated systems according to the MsM procedure (see Fig. 1).

Finally, the bulk properties of each pure component of the diverse PNCs listed in Table 3 constituted the last information necessary to run FEM calculations. All listed data were obtained from literature.[40] Thermal conductivities of MMT, BOE, SEP and HT were assumed to be the same and equal to the value found for bentonite clay.[40i] As each nanofiller itself was considered to be impermeable to gases, a very low permeability value (*i.e.*, $P = 0.0001$ barrer, see Table 3) was selected.

It is worth noticing here that the high-quality mesh generation is of fundamental importance in order to calculate realistic values of the macroscopic properties of the nanocomposite materials.

Table 3 Macroscopic properties of all PNC pure components: Young's modulus (E, GPa), Poisson ratio (ν), thermal conductivity (κ, W m^{-1} K^{-1}), and gas permeability (P, barrer)

	PP	PA6	TPU	MMT
E	1.55 (ref. 40*a*)	2.80 (ref. 40*e*)	0.02 (ref. 40*g*)	178 (ref. 40*h*)
ν	0.36 (ref. 40*b*)	0.35 (ref. 40*b*)	0.45 (ref. 40*b*)	0.2 (ref. 40*h*)
κ	0.25 (ref. 40*c*)	0.28 (ref. 40*f*)	0.20 (ref. 40*f*)	1.14 (ref. 40*i*)
P_{O2}	9.6 (ref. 40*d*)	4.7 (ref. 40*d*)	2.1 (ref. 40*d*)	10^{-4}
	TiO_2	SEP	BOE	HT
E	230 (ref. 40*j*)	200 (ref. 40*l*)	253 (ref. 40*m*)	139 (ref. 40*n*)
ν	0.25 (ref. 40*j*)	0.2 (ref. 40*l*)	0.20 (ref. 40*m*)	0.30 (ref. 40*n*)
κ	11.7 (ref. 40*k*)	1.14 (ref. 40*i*)	1.14 (ref. 40*i*)	1.14 (ref. 40*i*)
P_{O2}	10^{-4}	10^{-4}	10^{-4}	10^{-4}

Since a thorough discussion on this topic is beyond the main scope of the present paper, the interested reader is referred to another paper from our group dealing with this issue in detail.[26k]

3 Results and discussion

3.1 Atomistic MD simulations

Interaction energies, basal spacing values d for intercalated PNCs, and density profiles are all major information gathered from atomistic MD simulations and necessary for running next-level (*i.e.*, mesoscopic) simulations, as mentioned in the foregoing paragraphs. Further quantitative interfacial properties can be derived from atomistic MD simulations (*e.g.*, cleavage energies and packing constraints) which will be incorporated in a more refined model in our next work. Table 4 presents the binding energies between the individual PNC components obtained from the corresponding NVT MD simulations. An analysis of the values reported in this table leads to several, interesting observations, as follows. As somewhat expected, the presence of a modifier on the nanoparticle surface always results in a decrease of the interaction energy between the polymer and nanofillers itself. Indeed, the values $E_{NF/P}$ for the systems devoid of surface modifiers are all above 100 kcal mol^{-1}, while substantially lower values are estimated for those PNCs with surface-modified nanoparticles.

As found in previous studies,[26c,d,41] the binding energy between a polymer/surface-modified nanofillers couple strongly depends upon the volume of an organic modifier and the eventual presence of polar groups in its chain(s) (see the last column of Table 4). Definitely, the atomistic binding energies estimated in this work for both PP and PA6 confirm this trend (see Table 4). A significant exception is constituted by the system PP/ODA, a finding easily rationalized considering the substantially apolar nature and small dimension of ODA which, in turn, exert a low influence on the interactions between the polymer and the filler.[26c,d]

In the case of PP/MMT-based PNCs, we also found that the mineral CEC exerts a significant effect on the energetics of the

Table 4 Binding energies between the individual PNC components obtained from atomistic MD simulations. All energies are in kcal mol^{-1}

System	$E_{NF/P}$[a]	$E_{NF/SM}$[b]	$E_{P/SM}$[c]	V^d/Å^3
PP/C10A	75	394	94	483
PP/C15A	25	854	131	735
PP/C20A	47	440	99	735
PP/C30B	85	418	99	470
PP/ODA	120	293	66	345
PA6/C20A	6	475	155	735
PA6/C30B	27	433	156	470
PA6/M_3C_{18}	33	444	163	383
TPU/C30B	95	384	143	470
PP/HT/FA	52	1925	100	314 (C_{16}) 346 (C_{18})
PP/SEP	102	—	—	—
PP/BOE	172	—	—	—
PP/TiO_2	102	—	—	—

[a] $E_{NF/P}$ = interaction energy between the nanofillers and the polymer. [b] $E_{NF/SM}$ = interaction energy between the nanofillers and the surface modifier. [c] $E_{P/SM}$ = interaction energy between the polymer and the surface modifier. [d] V = molecular volume of the surface modifier.

corresponding systems. In fact, when the MMT CEC is higher (*i.e.*, system PP/C15A), the binding energy values clearly reveal stronger interactions between polymer and organic modifiers, and MMT and organic modifiers, respectively, while the interactions between the nanofillers and the polymer are hindered due to the crowding of the organics on the MMT surface which leaves less free space for polymer/filler favourable contacts.

The nature of the bonds between the surface modifiers and the nanofillers for all PP/MMT, PP/HT, PA6/MMT, and TPU/MMT systems analysed is ionic. Thus, it is not surprising that for all these PNCs the binding energies $E_{NF/SM}$ are significantly higher than the values of $E_{NF/P}$ and $E_{P/SM}$, respectively. Also, since HT is characterized by a high charge density in the interlayer space, this last property can be invoked to support the evidence that the binding energy $E_{NF/SM}$ for the system PP/HT is quite higher (1925 kcal mol^{-1}) than the corresponding MMT-based systems (see Table 4).

Interestingly, no major differences were observed in those systems containing pristine nanofillers. In all these cases, since the interactions between the nanoparticles and the polymeric chains are mainly determined by van der Waals interactions, the corresponding values of $E_{NF/P}$ are comparable, the one for the PP/BOE system being slightly higher than the other two PNCs (PP/TiO_2 and PP/SEP, respectively).

Table 5 lists the predicted interlayer distance values d for all intercalated PNCs considered in this work, as obtained from the corresponding atomistic NPT MD simulations. Intuitively, an organic surface modifier characterized by larger molecular dimensions (see the last column of Table 4) induces a larger inter-gallery distance in the corresponding modified mineral. More important, perhaps, is the good agreement of the *in silico d* values with the corresponding experimental results[26e,37,42,43] (shown in parenthesis in Table 5 for comparison), since this quantity constitutes a direct input parameter for the successive, *i.e.*, mesoscopic, set of simulations.

3.2 Mesoscale simulations

The application of computer-based simulation techniques at the mesoscale level aims both at filling the gap between detailed atomistic and coarse continuum level, and to avoid their shortcomings. In the specific field of PNCs, mesoscale simulations are employed to study the structural evolution, the microphase structure and the phase separation of these systems.[26] Fig. 2 shows an illustration of the equilibrated model obtained from DPD simulations of the PP/HT/FA PCN system as an example.

In order to validate our mesoscale level calculations, performed using parameters generated *via* a mapping procedure based on the information stemming from the lower scale MD simulations, we chose to compare the number density profiles calculated from MD trajectories with those obtained by analysis of the DPD runs. The density profiles capture the arrangement of the total organic matter (polymer and surface modifiers) in the mineral galleries, through a plane normal to the galleries (z-direction). In the case of polymer-intercalated clay stacks, there is a general agreement amongst researchers about the arrangement of organic species within the gallery systems:[26e,i,44,45] intercalated species usually exhibit high and low density layers alternating from the clay surface, rapidly reaching bulk polymer density in the centre of the gallery. This arrangement was indeed confirmed by the distribution of the organic density obtained from both MD and DPD simulations, as shown in Fig. 3 again for the system PP/HT/FA PCN as an example.

As we can see from Fig. 3, the system organizes into layers inside the clay gallery. This layering effect is well-known for confined liquids,[46–48] and arises mainly from solvation forces. The rough and irregular shape of the profile obtained for confined macromolecules—if compared, for instance, to the smooth and regular one exhibited by low molecular weight confined fluids—is due to the additional constraints to which the polymer atoms are subjected, as being connected along chains that run across many adjacent organic layers. However, Fig. 3 clearly shows that the peaks have different heights and widths, depending on their location within the gallery. The highest density peaks are those closer to the clay layers; their height is indicative of the strong affinity between the adsorbed organic/polymer chains and the clay surface.[26i,k,49,50] The adjacent peaks are lower, as a consequence of the adsorption of the first layer that partially shields the attractive potential of the clay surface. In the centre of the gallery, practically only polymer chains are found. Since the overall arrangement and, in particular, the

Table 5 Basal spacing of stacks in intercalated PNCs calculated by MD simulations. Available experimental data are reported in parenthesis, for comparison

Stack	Interlayer spacing/nm
PP/C10A	3.73 (3.71, ref. 42)
PP/C15A	4.90
PP/C20A	4.10
PP/C30B	3.68
PP/ODA	3.73
PA6/C20A	4.22 (4.22, ref. 43)
PA6/M_3C_{18}	4.00
PA6/C30B	4.22
TPU/C30B	4.22
PP/HT/FA	4.10 (4.1, ref. 37)

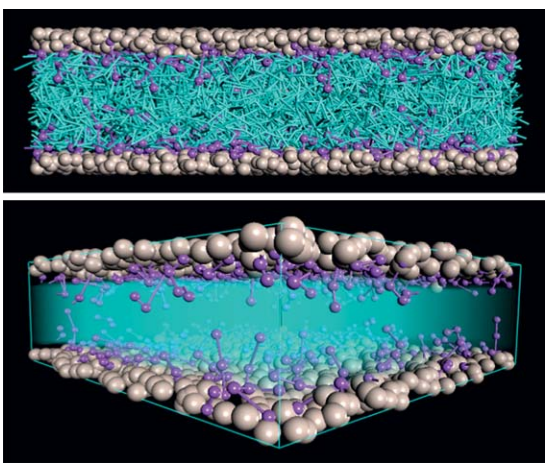

Fig. 2 Front (top) and side (bottom) views of the equilibrated mesoscopic model obtained from DPD simulations of the PP/HT/FA PNC system. Colour code: gray, HT; purple, FA; light blue, PP. In the bottom panel, the PP beads are replaced by a light blue field, to highlight the distribution of the FA molecules within the HT layers.

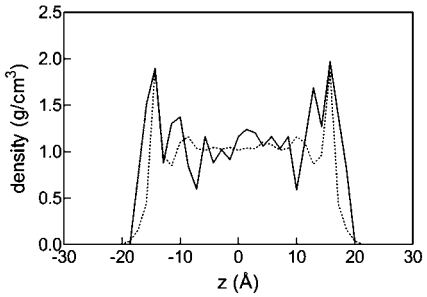

Fig. 3 Comparison between interlayer densities of organic species (surface modifiers and polymer) in the gallery space of the PP/HT/FA PCN as obtained from MD (continuous line) and DPD (dotted line) simulations, respectively.

presence of high density peaks next to the clay surface are in agreement with the current literature on similar systems,[51–53] this evidence constitutes a further confirmation that the adopted atomistic/mesoscopic mapping procedure correctly reproduces density distributions of polymer chains and surface modifier molecules within inorganic layers.

For the PNCs with pristine nanofillers, the arrangement of the DPD polymer beads near the different inorganic surfaces reflects the trends determined by atomistic MD calculations as well. Interestingly, the partial adsorption of the polymer molecules onto the filler surface results in the development of a polymer layer, as evidenced by the corresponding density maps (see Fig. 4) which, in principle, might have properties different from those of the bulk polymer matrix.[54] The thickness of this interphase, as expected, depends on the type and strength of the interaction between the nanoparticle surface and the polymer, being usually generated by secondary van der Waals or electrostatic forces. Thus, values from 1 nm to several microns have been reported in the literature for the most diverse PNCs.[55] As can be inferred from Fig. 4, the interphase thicknesses obtained from our mesoscopic simulations for the BOE, SEP and TiO_2 PNCs are similar, the one for the TiO_2-based system ($\sim$1.7 nm) being slightly larger than that estimated for the BOE and SEP PNCs (1.1–1.2 nm). Interestingly, these values are in line with experimental evidence available on similar systems.[55]

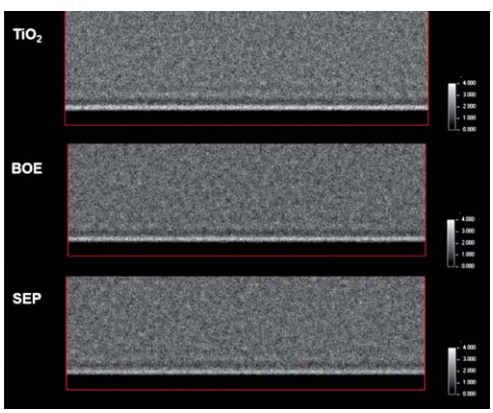

Fig. 4 Mesoscopic density maps obtained for TiO_2- (top), BOE- (centre), and SEP- (bottom) based systems.

3.3 MicroFEM calculations of stack properties for intercalated PNCs

To calculate a set of macroscopic properties of a PNC stack (see Fig. 5), we resorted to finite-element fixed-grid (*MesoProp*) calculations. In particular, the Young's modulus E, the thermal conductivity κ, and the gas permeability P were the macroscopic properties of election, since not only these quantities are of primary industrial interest but, perhaps more importantly, direct comparison with the corresponding experimental data could be made.[37]

Aside pure component properties, the mesoscopic density matrices obtained from DPD simulations for each PNC system were used as input information as well. We must note here that, for permeability, a value of $P = 0.0001$ barrer was chosen for the MMT and HT platelets, as the stacks were reasonably assumed to be non-permeable to gases. All relevant results are presented in Table 6. Each property is expressed as an average value in the x and y directions with respect to the orientation of the platelets.

3.4 MicroFEM calculations of the properties for unmodified PNCs with interfaces

As briefly mentioned above, non-treated fillers have high energy surfaces. Accordingly, during the most common PNC preparation process (*i.e.*, melt mixing), intermolecular forces lead to a partial adsorption of polymer chains onto the filler surfaces. The thickness and the properties of the resulting interphase have not been indisputably unveiled so far. Indeed, if the formation of a softer interphase was claimed by some authors, other, more frequent reports reveal the presence of a stiffer interface which, in turn, contributes to the overall increase of the PNC stiffness. In order to account for the existence of this interphase in our surface-pristine PNCs, we performed *MesoProp* fixed-grid calculations using the corresponding DPD density maps (see Fig. 4) as input. With this information on hand, we then estimated the properties of the corresponding pseudo-"core–shell" model nanoparticles as listed in Table 7. Finally, these values were employed in the last FEM calculations, yielding the overall macroscopic properties of each corresponding PNC.

3.5 Macroscopic properties of all nanocomposite systems

The prediction of the macroscopic properties of the entire polymer nanocomposite systems was achieved with FEM calculations using a variable-grid approach.[56] In the case of surface-modified nanoparticle PNCs, a cell was created and objects as single platelets and stacks were added until the required volume fraction was achieved. Fig. 6 shows the FEM model adopted for the PP/HT/FA PNC system as an example.

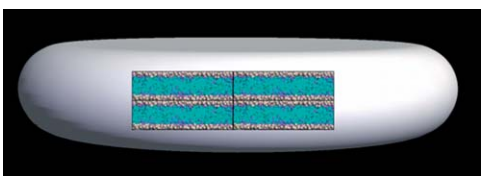

Fig. 5 Example of the intercalated stack model for the PP/HT/FA PNC system used in the FE calculations.

Table 6 Properties of intercalated PNC stacks estimated using fixed-grid calculations performed exploiting the density profiles of each system derived from mesoscale simulations. Symbols: E = Young's modulus; κ = thermal conductivity; P = permeability. Standard deviations are given in parenthesis

Stack	E/GPa	κ/W m^{-1} K^{-1}	P_{O2}/barrer
PP/C10A	70.06 (0.19)	1.070 (0.076)	1.69×10^{-3} (1.1×10^{-4})
PP/C15A	75.44 (0.43)	1.092 (0.079)	1.93×10^{-3} (1.3×10^{-4})
PP/C20A	72.36 (0.70)	1.078 (0.078)	1.84×10^{-3} (1.1×10^{-4})
PP/C30B	70.34 (0.57)	1.070 (0.075)	1.74×10^{-3} (1.2×10^{-4})
PP/ODA	88.22 (0.46)	1.186 (0.090)	1.32×10^{-3} (1.1×10^{-4})
PA6/C20A	110.30 (0.07)	1.298 (0.080)	9.00×10^{-4} (0.95×10^{-4})
PA6/M3C18	110.39 (0.15)	1.295 (0.083)	8.20×10^{-4} (0.89×10^{-4})
PA6/C30B	110.30 (0.12)	1.295 (0.082)	8.60×10^{-4} (0.91×10^{-4})
TPU/C30B	100.05 (0.11)	1.088 (0.112)	4.02×10^{-4} (0.44×10^{-4})
PP/HT/FA	104.22 (0.15)	1.283 (0.080)	5.64×10^{-3} (1.3×10^{-4})

Table 7 Properties of nanoparticles with interfaces estimated using the interface thickness and properties inferred from mesoscale and fixed-grid simulations. Standard deviations are given in parenthesis

PNC	E/GPa	κ/W m^{-1} K^{-1}	$P(O_2)$/barrer
PP/BOE	241.89 (0.22)	1.130 (0.08)	0.97 (0.11)
PP/SEP	152.07 (0.30)	1.070 (0.06)	4.93 (0.61)
PP/TiO_2	172.75 (0.26)	8.94 (0.45)	4.73 (0.62)

The properties of pure components (polymers, MMT and HT) were inserted in materials database together with the properties of the stacks as obtained using the fixed-grid (*MesoProp*) calculations described above. On the other hand, in the case of the system without organic modifiers the cell was generated using the pseudo-"core–shell" filler models, and assigning to these the corresponding values listed in Table 7.

The set of properties and their values calculated for all the different nanocomposite systems are shown in Fig. 7 in terms of enhancement factor $E_f = P_c/P_m$, *i.e.*, the ratio between a given property value for the nanocomposite (P_c) and the corresponding value for the pristine polymer matrix (P_m).

3.5.1 Intercalated systems. In general, an increase of 60% on mechanical properties is observed when a 4.6% w/w of MMT is added to PP or PA6 matrices. Since the elastic modulus of neat PP is lower than that of PA6, FEM calculations show that the elastic modulus of the PA6/MMT nanocomposites is also slightly higher than that of PP/MMT systems (see Fig. 7), which can be further attributed to the higher mechanical properties of PA6/MMT stacks with respect to the corresponding PP/MMT counterparts (Table 6).

According to fixed-grid calculations, substituting MMT with HT in PP-based PNCs results in PP/HT stacks with higher elastic modulus than the PP/MMT stacks (see Table 6). This enhancement can be due to the high affinity between PP chains and HT platelets, as testified by the low value of the DPD interaction parameter $a_{M/P}$ for the PP/HT system (see Table 2). Notwithstanding, a moderate increase in mechanical property is predicted in the case of PP/HT PNC, as a result of the low elastic modulus of pristine hydrotalcite. It is well known that intercalation of HT is linked with difficulties due to the high charge interlayer density, which leads to strong electrostatic interactions between the sheets. Experimental trials to produce this kind of nanocomposites showed that HT particles of 10 μm tend to de-agglomerate into smaller, disk-like aggregates with diameters ranging from 200 to 500 nm and consisting of 3–4 layers of layered double hydroxides.[57] De-agglomeration, poor dispersion and different aspect ratios are usually invoked to explain the high range of variability in the enhancement factor of the Young's modulus of these nanocomposites (*e.g.*, from 1.07 for 10% w/w of HT[37] to 1.28 for 3% w/w of HT[58]). Taking all these aspects into account, our estimated value of $E_f = 1.29$ for the 4.6% w/w proves the predictive character of our multiscale approach.

Neat TPU has an elastic modulus significantly lower than the other polymers considered (Table 3). Interestingly, reinforcing this low-modulus matrix with nanofillers has the highest beneficial effect which, in turn, reflects in the highest increase in the Young's modulus of the relevant TPU/MMT PNC with respect to all other intercalated PNCs (Fig. 7).

Concerning the other macroscopic properties considered, an increase of about 10% in thermal conductivity and a decrease of ~25% (PP) and 36% (PA6) in permeability are predicted by our MsM approach. The gas permeability in a PNC depends mainly on orientation, aspect ratio and volume fraction of the filler in the matrix. A rationale for the fact that the PA6/MMT nanocomposite systems offer a higher barrier to the diffusion of gas with respect to the PP-based nanocomposites (Fig. 4) can be based on the fact that both (i) the volume fraction of MMT in the PA6 matrix and (ii) the density of PA6 polymer are higher than those of PP. Other differences might be noted depending on the surface modifiers used which, in turn, stem from the diverse stack properties and dissimilar aspect ratios.

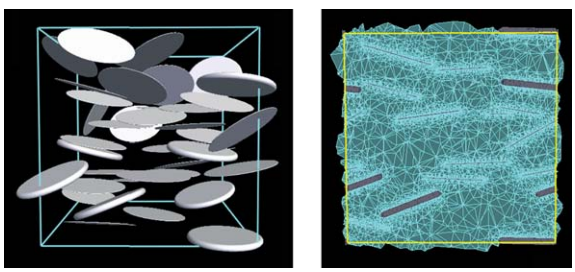

Fig. 6 Global model configuration (left) and relative meshed volume (right) used in the FE calculations for the PP/HT/FA PNC system.

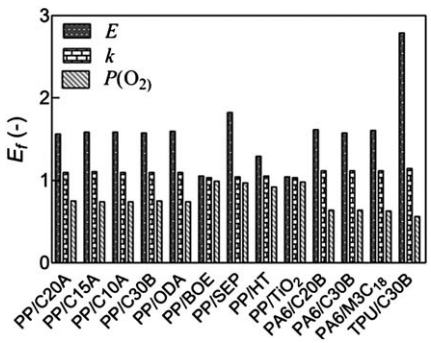

Fig. 7 Predicted enhancement factor $E_f = P_c/P_m$ of the macroscopic properties of different nanocomposite systems.

A series of different measurements and morphological characterizations were reported by Fornes *et al.*[59] in a complex and elegant study where sodium montmorillonite was modified with a series of organic amine salts. Interestingly, a good agreement is found between the experimental data of Fornes and the present results in a direct comparison for PA6-based nanocomposite systems with Φ_w = 4.5% w/w. Indeed, the experimental enhancement factors E_f of 1.57, 1.62 and 1.69 for the Young's modulus E of the systems PA6/C20A, PA6/C30B, and PA6/M_3C_{18} quite nicely correspond to our calculated values of 1.61, 1.57, and 1.60, respectively. In the case of the PA6/C30B and PA6/M_3C_{18} systems, the calculated E_f values are somewhat lower than those obtained by simulation. These small discrepancies can be justified by considering the very high level of exfoliation and dispersion of the MMT platelets in the experimental samples.[59] However, it is clear that the system with M_3C_{18} as clay modifier yields a greater enhancement in Young's modulus than the C30B composite according to both simulated and experimental results. On the other hand, our simulations show that PA6/C20A offers the highest increase of the Young's modulus, which is not supported by experiments due to the partial intercalation that takes place by using this kind of surfactants.[59]

In the case of TPU-based nanocomposites, a good agreement of the predicted Young's modulus is found with the experimental results,[46] since an E_f value of 2.96 for TPU loaded with 5% w/w of C30B compares well with the *in silico* value of 2.76. For the same system, also the experimental E_f = 1.18 for thermal conductivity[40f] quite nicely matches the predicted value of 1.14. It is important to note here that a substantially higher increase in the conductivity value along the x and y directions with respect to the z direction was observed, which was due to the alignment of the platelets on those directions.

Lastly, given the small difference between calculated and experimental κ values (approximately 3.5%), we can state that the predictive power of the multiscale procedure is validated also for this property.

3.5.2 PNC systems without surface modifiers. Recently, in the framework of the jointed European integrated project (IP) *Multihybrids*, Tabuani *et al.*[37] experimentally evaluated the mechanical properties of the same series of pristine PNCs based on SEP, BOE, MMT, and HT. In the case of PP/SEP nanocomposite, our calculated enhancement factor for the Young's modulus E_f = 1.47 is in an excellent agreement with the experimental values of 1.46 (ref. 37) and 1.50.[60] Fig. 8 illustrates the FE model used for the prediction of the mechanical properties of the PP/SEP PNC.

Due to the incomplete dispersion/agglomeration of the filler which takes place during processing, the PP/BOE system was defined considering agglomerates of spherical shape (see ESI‡ for details). Fig. 9 shows a comparison between the TEM images of the PP/BOE PNC agglomerates[61] and our simulated system. The corresponding, predicted Young's modulus (E_f = 1.05) is slightly lower than the available experimental values (E_f = 1.11 (ref. 49) and 1.18 (ref. 37)), due to (a) the definition of the filler as a spherical object in a trial approximation of the real shape of the aggregates (see Fig. 9) and (b) the somewhat different volume fraction employed in the real PNC (5 *vs.* 4.6% w/w). Notwithstanding the degree of approximation, our computational

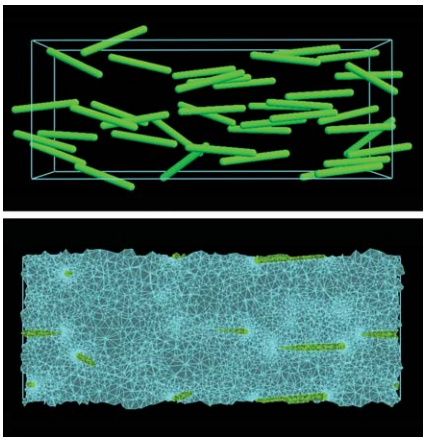

Fig. 8 (Top) FEM PP/SEP model and (bottom) the corresponding FEM mesh.

predictions and the relevant experimental results can be considered to be in very good agreement.

The lowest increase in elastic modulus E for the entire set of PNCs considered in this work was observed for those systems loaded with spherical fillers, as exemplified by the modest 4% increase of the Young's modulus E for the PP/TiO_2 system (see Fig. 7 and 10).

An experimental characterization of the dimensions of titania nanoparticles performed again in the Multihybrids IP framework[39] revealed quite a broad distribution (10–100 nm), with a marked peak centred around 20 nm. Although no experimental E_f values are available for this system, the MsM procedure predicts a reliable increase of ~3.4% in the thermal conductivity κ and a concomitant decrease of 2% in the oxygen permeability P_{O2}. Based on the results obtained for the PP/TiO_2 and PP/BOE PNCs we can conclude that, as intuitively expected by virtue of the low aspect ratio, spherical nanofillers exert a limited influence

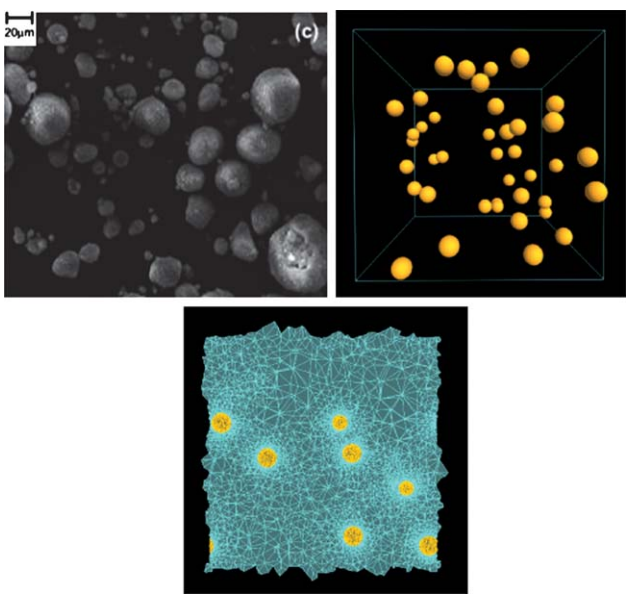

Fig. 9 (Top, left) SEM image of PP/BOE PNC agglomerates studied in this work.[61] (Top, right) FEM PP/BOE model and (bottom) the corresponding FEM mesh.

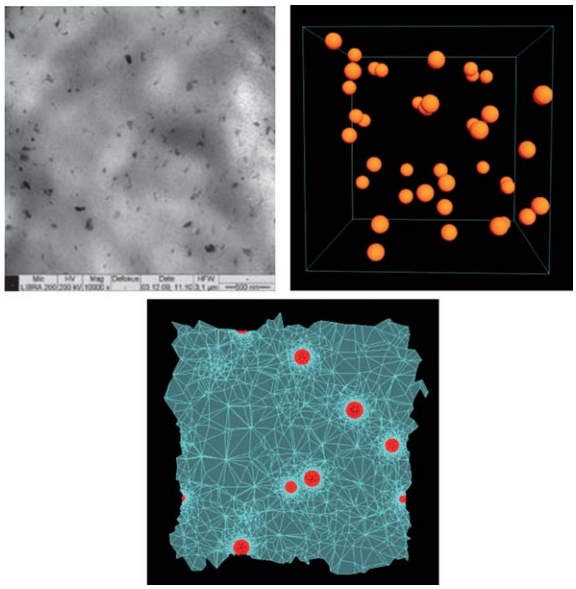

Fig. 10 (Top, left) TEM image of the PP/TiO_2 PNC studied in this work.[39] (Top, right) FEM PP/TiO_2 model and (bottom) the corresponding FEM model mesh.

on the thermophysical properties of the corresponding polymer nanocomposites.

From a general perspective, our calculations confirm and substantiate the general assumption that aspect ratio and/or shape of the filler significantly influence the mechanical properties of polymer-based nanocomposites. In our comprehensive study, fibres (*i.e.*, sepiolite) and platelets in the system TPU/C30B significantly offer the highest E_f in terms of mechanical behaviour (see Fig. 7). In the first case, this increment is clearly induced by the shape and aspect ratio of the filler, while in the second case it is the very low Young's modulus of the pristine TPU polymer that plays a fundamental role in the enhancement of the value of E (Table 3). On the other hand, the lowest increase (<10%) in the mechanical properties is observed for those systems with spherical fillers (PP/BOE and PP/TiO_2), while platelet-based PNCs show a considerable increase up to 60% for MMT-based PNCs. Also, the presence and the different nature of small organics as surface modifiers may ultimately contribute—although to a more limited extent—to the overall improvement of the PNC mechanical performances.

Concerning thermal conductivity, even if no substantial differences were predicted among the different PNCs considered, some global conclusions can be presented. Even if the thermal conductivity of TiO_2 is quite high with respect to the other fillers (see Table 3), no significant increase in the κ value for the corresponding PP/TiO_2 PNC is observed. A similar value of E_f for thermal conductivity is predicted for another system with spherical filler (PP/BOE), even if the thermal conductivity of boehmite is significantly lower than that of TiO_2 (Table 3). Coupled together, this evidence allows us to conclude that spherical fillers exert an overall negligible effect also on the thermal conductivity of the respective PNCs.

Lastly, as far as oxygen permeability is concerned, a pronounced decrease in P is observed in the case of intercalated nanocomposites (see Fig. 7) with respect to all other PNCs (SEP, BOE, and TiO_2), which are more or less dispersed. A decrease of 25% and 36% in permeability is predicted for intercalated systems with PP and PA6, respectively, while the effect is confined to less than 3% in all other cases. Based on these results it is evident that permeability strongly depends on the internal morphology and alignment of the fillers in the polymer matrix, more ordered (intercalated) arrangement of filler featuring the higher decrease in permeability.

4 Conclusions

In this paper we presented the development and application of a multiscale molecular modelling (MsM) procedure for the prediction of the macroscopic properties of polymer-based nanocomposites. The results obtained from this *in silico* approach are very encouraging, as the predicted values for a selected set of thermophysical quantities are in outstanding agreement with the corresponding experimental counterparts. Moreover, the analysis of the entire panel of results allowed us to draw some general conclusions regarding the role of the single components with respect to the overall performance of the different PNCs. First, the presence of modifiers on the surface of the nanoparticles has a significant effect on the interactions between the polymeric matrix and the nanofiller which may reflect a great influence on the intercalation/exfoliation process during the preparation of PNC. This, in turn, affects the overall structure of the nanocomposite and, ultimately, its macroscopic property. However, once a specific morphology is generated at the nanoscale level, the chemical/physical characteristics of the different surface modifiers are smeared out, and their individual contribution to the PNC macroscopic properties becomes negligible. On the other hand, the size and shape of the filler as well as the properties of the pure nanocomposite components are all aspects that have a big impact on overall material properties.

Spherical fillers affect mechanical and other thermal properties to a minimum extent, independently on nanoparticle dimensions. On the opposite, the impact of high aspect ratio nanoparticles such as fibres is significantly higher, and it can be further influenced by the change in fibre length or orientation within the polymeric matrix. In the case of clay, the aspect ratio of the platelets plays a key role in determining the ultimate properties of the relevant nanocomposites, as also confirmed by our previous studies in which we examined the effect of the different degrees of exfoliation in polymer/MMT nanocomposites.[26k] Quite intuitively, the best exfoliated structures result in the most enhanced mechanical properties.

Within the framework of our current material science and engineering research, we can conclude that a complete integration of all available simulation scales (*i.e.*, from atomistic molecular simulations *via* mesoscopic dynamics to finite element calculations) in a hierarchical procedure such as that proposed in the present work can be a very useful tool for the morphological investigation of polymer-based nanocomposites and the *a priori* prediction of the ultimate properties of these fascinating materials. Undoubtedly, further work is necessary to achieve a more refined multiscale integration for these materials; however, the simple approach proposed in this paper represents, at least in our opinion, the best compromise between the overall computational

time required to carry out the entire multiscale molecular modeling procedure and the great quality of the results predicted.

Acknowledgements

All authors gratefully acknowledge the generous financial support to their work received in the framework of the 6th European Commission Framework Program Integrated Project "*MultiHybrids*" (grant 026685-2IP). DRN also wishes to acknowledge the financial support from CONACYT Mexico (grant no. 146624).

Notes and references

1 A. Convertino, G. Leo, M. Striccoli, G. Di Marco and M. L. Curri, *Polymer*, 2008, **49**, 5526–5532.
2 J. N. Coleman, U. Khan, J. W. Blau and Y. K. Gunko, *Carbon*, 2006, **44**, 1624–1652.
3 S. S. Ray and M. Okamoto, *Prog. Polym. Sci.*, 2003, **28**, 1539–1641.
4 K. Chrissopoulou and S. H. Anastasiadis, *Eur. Polym. J.*, 2011, **47**, 600–613.
5 S. P. Lonkar, S. Therias, N. Caperaa, F. Leroux and J. L. Gardette, *Eur. Polym. J.*, 2010, **46**, 1456–1464.
6 S. Xie, S. Zhang, F. Wang, M. Yang, R. Seguela and J. M. Lefebvre, *Compos. Sci. Technol.*, 2007, **67**, 2334–2341.
7 Y. Xu and Y. V. Hoa, *Compos. Sci. Technol.*, 2008, **68**, 854–861.
8 S. Pavlidou and C. D. Papaspyrides, *Prog. Polym. Sci.*, 2008, **33**, 1119–1198.
9 G. Choudalakis and A. D. Gotsis, *Eur. Polym. J.*, 2009, **45**, 967–984.
10 C. J. Wu, A. K. Gaharwar, P. J. Schexnailder and G. Schmidt, *Materials*, 2010, **3**, 2986–3005.
11 Q. H. Zeng, A. B. Yu and G. Q. Lu, *Prog. Polym. Sci.*, 2008, **33**, 191–269.
12 M. Alexandre and P. Dubois, *Mater. Sci. Eng., R*, 2000, **28**, 1–63.
13 R. P. Feynman, *Engineering and Science*, 1960, **23**, 22–36.
14 S. A. Baeurle, *J. Math. Chem.*, 2009, **46**, 363–426.
15 B. Minisini and F. Tsobnang, *Composites, Part A*, 2005, **36**, 539–544.
16 G. Allegra, G. Raos and M. Vacatello, *Prog. Polym. Sci.*, 2008, **33**, 683–731.
17 H. W. Wang, H. W. Zhou, R. D. Peng and L. Mishnaevsky, Jr, *Compos. Sci. Technol.*, 2011, **71**, 980–988.
18 N. Sheng, M. C. Boyce, D. M. Parks, G. C. Rutledge, J. L. Abes and R. E. Cohen, *Polymer*, 2004, **45**, 487–506.
19 P. D. Spanos and A. Kontsos, *Probab. Eng. Mech.*, 2008, **23**, 456–470.
20 C. Li and T. W. Chou, *Compos. Sci. Technol.*, 2006, **66**, 2409–2414.
21 D. Luo, W. X. Wang and Y. Takao, *Compos. Sci. Technol.*, 2007, **67**, 2947–2958.
22 A. Jafari, A. A. Khatibi and M. M. Mashhadi, *Composites, Part B*, 2011, **42**, 553–561.
23 Z. Boming, Y. Zhong, W. Yufeng and S. Hongwei, *Mater. Des.*, 2010, **31**, 2312–2318.
24 V. Sansalone, P. Trovalusci and F. Cleri, *Acta Mater.*, 2006, **54**, 3485–3492.
25 K. Matous, H. M. Inglis, X. Gu, D. Rypl, T. L. Jackson and P. H. Geubelle, *Compos. Sci. Technol.*, 2007, **67**, 1694–1708.
26 (*a*) M. Fermeglia, M. Ferrone and S. Pricl, *Fluid Phase Equilib.*, 2003, **212**, 315–329; (*b*) M. Fermeglia, M. Ferrone and S. Pricl, *Mol. Simul.*, 2004, **30**, 289–300; (*c*) R. Toth, A. Coslanich, M. Ferrone, M. Fermeglia, S. Pricl, S. Miertus and E. Chiellini, *Polymer*, 2004, **45**, 8075–8083; (*d*) R. Toth, M. Ferrone, S. Miertus, E. Chiellini, M. Fermeglia and S. Pricl, *Biomacromolecules*, 2006, **7**, 1714–1719; (*e*) G. Scocchi, P. Posocco, M. Fermeglia and S. Pricl, *J. Phys. Chem. B*, 2007, **111**, 2143–2151; (*f*) P. Cosoli, G. Scocchi, S. Pricl and M. Fermeglia, *Microporous Mesoporous Mater.*, 2008, **107**, 169–179; (*g*) M. Fermeglia and S. Pricl, *Prog. Org. Coat.*, 2007, **5**, 187–199; (*h*) M. Fermeglia, P. Cosoli, M. Ferrone, S. Piccarolo, G. Mensitieri and S. Pricl, *Polymer*, 2006, **47**, 5979–5989; (*i*) R. Toth, D. J. Voorn, J. W. Handgraaf, J. G. E. M. Fraaije, M. Fermeglia, S. Pricl and P. Posocco, *Macromolecules*, 2009, **42**, 8260–8270; (*j*) G. Scocchi, P. Posocco, A. Danani, S. Pricl and M. Fermeglia, *Fluid Phase Equilib.*, 2007, **261**, 366–374; (*k*) S. P. Pereira, G. Scocchi, R. Toth, P. Posocco, D. R. Nieto, F. Santese, S. Pricl and M. Fermeglia, *Journal of Multiscale Modeling*, 2011, **3**, 11–26; (*l*) G. Scocchi, P. Posocco, J. W. Handgraaf, J. G. E. M. Fraaije, M. Fermeglia and S. Pricl, *Chem.–Eur. J.*, 2009, **15**, 7586–7592; (*m*) P. Posocco, Z. Posel, M. Fermeglia, M. Lísal and S. Pricl, *J. Mater. Chem.*, 2010, **20**, 10511–10520; (*n*) M. Maly, P. Posocco, S. Pricl and M. Fermeglia, *Ind. Eng. Chem. Res.*, 2008, **47**, 5023–5038.
27 (*a*) H. Zhang, X. Lu, Y. Leng, L. Fang, S. Qu, B. Feng and J. W. J. Wang, *Acta Biomater.*, 2009, **5**, 1169–1181; (*b*) S. Sutton and G. Sposito, *Geochim. Cosmochim. Acta*, 2006, **70**, 3566–3581; (*c*) Y. Han and J. Elliott, *Comput. Mater. Sci.*, 2007, **39**, 315–323.
28 H. Sun, *J. Phys. Chem. B*, 1998, **102**, 7338–7364.
29 D. Rigby, *Fluid Phase Equilib.*, 2004, **217**, 77–87.
30 M. Bellotto, B. Rebours, O. Clause and J. Lynch, *J. Phys. Chem.*, 1996, **100**, 8527–8534.
31 M. Fermeglia and S. Pricl, *AIChE J.*, 1999, **45**, 2619–2627.
32 (*a*) P. J. Hoogerbruge and J. M. V. A. Koelman, *Europhys. Lett.*, 1992, **18**, 155–160; (*b*) J. M. V. A. Koelman and P. J. Hoogerbruge, *Europhys. Lett.*, 1993, **21**, 363–368; (*c*) R. D. Groot and P. B. Warren, *J. Chem. Phys.*, 1997, **107**, 4423–4435.
33 (*a*) P. Posocco, M. Fermeglia and S. Pricl, *J. Mater. Chem.*, 2010, **20**, 7742–7753; (*b*) P. Posocco, S. Pricl, S. P. Jones, A. Barnard and D. K. Smith, *Chem. Sci.*, 2010, **1**, 393–404; (*c*) S. P. Jones, N. P. Gabrielson, C. H. Wong, H. F. Chow, D. W. Pack, P. Posocco, M. Fermeglia, S. Pricl and D. K. Smith, *Mol. Pharmaceutics*, 2011, **8**, 416–429; (*d*) A. Barnard, P. Posocco, S. Pricl, M. Calderon, R. Haag, M. E. Hwang, V. W. T. Shum, D. W. Pack and D. K. Smith, *J. Am. Chem. Soc.*, 2011, **133**, 20288–20300.
34 M. A. Osman, V. Mittal and H. R. Lusti, *Macromol. Rapid Commun.*, 2004, **25**, 1145–1149.
35 M. Heggli, T. Etter, P. Wyss, P. J. Uggowitzer and A. A. Gusev, *Adv. Eng. Mater.*, 2005, **7**, 225–229.
36 A. A. Gusev, *J. Mech. Phys. Solids*, 1997, **45**, 1449–1459.
37 D. Tabuani, S. Ceccia and G. Camino, *Macromol. Symp.*, 2011, **301**, 114–127.
38 R. C. Streller, R. Thomann, O. Torno and R. Mulhaupt, *Macromol. Mater. Eng.*, 2008, **293**, 218–227.
39 6th EC FP IP *MultiHybrids* (026685-2IP) project consortium, private communication, 2011.
40 (*a*) PP data sheet, https://polymers.lyondellbasell.com/; (*b*) R. J. Crawford, *Plastics Engineering*, Elsevier, 3rd edn, 1998; (*c*) Plastic materials database (IDES), http://www.ides.com; (*d*) L. K. Massey, *Permeability Properties of Plastics and Elastomers—A Guide to Packaging and Barrier Materials*, William Andrew Publishing/Plastics Design Library, 2nd edn, 2003; (*e*) PA6 data sheet, http://www.rhodia.com; (*f*) W. K. Ho, J. H. Koo and O. A. Ezekoye, *J. Nanomater.*, 2010, 1–11; (*g*) TPU data sheet, http://www.basf.com; (*h*) T. D. Fornes and D. R. Paul, *Polymer*, 2003, **44**, 4993–5013; (*i*) R. Almanza and M. C. Lozano, *Sol. Energy*, 1990, **45**, 241–245; (*j*) J. Winkler, Titanium Dioxide, in *European Coating Literature*, 2003; (*k*) http://www.ceram.com; (*l*) E. Bilotti, R. Zhang, H. Deng, F. Quero, H. R. Fischer and T. Peijs, *Compos. Sci. Technol.*, 2009, **69**, 2587–2595; (*m*) M. R. Gallas and G. J. Piermarini, *J. Am. Ceram. Soc.*, 1994, **77**, 2917–2920; (*n*) M. A. Thyveetil, P. V. Coveney, J. L. Suter and H. C. Greenwell, *Chem. Mater.*, 2007, **19**, 5510–5523.
41 (*a*) H. Heinz, H. Koerner, K. L. Anderson, R. A. Vaia and B. L. Farmer, *Chem. Mater.*, 2005, **17**, 5658–5669; (*b*) Y.-T. Fu and H. Heinz, *Chem. Mater.*, 2010, **22**, 1595–1605.
42 D. Marchant and K. Jayaraman, *Ind. Eng. Chem. Res.*, 2002, **41**, 6402–6408.
43 T. D. Fornes, D. L. Hunter and D. R. Paul, *Macromolecules*, 2004, **37**, 1793–1798.
44 F. Gardebien, A. Gaudel-Siri, J. L. Brédas and R. Lazzaroni, *J. Phys. Chem. B*, 2004, **108**, 10678–10686.
45 H. Heinz, R. A. Vaia, R. Krishnamoorti and B. L. Farmer, *Chem. Mater.*, 2007, **19**, 59–68.
46 J. N. Israelachvili, *Intermolecular and Surface Forces*, Academic Press, San Diego, CA, 1992.
47 S. Cui, P. T. Cummings and H. D. Cochran, *J. Chem. Phys.*, 2001, **114**, 7189–7194.
48 M. Fermeglia and S. Pricl, *Rheol. Acta*, 2001, **40**, 104–110.
49 I. Bitsanis and G. Hadziioannou, *J. Chem. Phys.*, 1990, **92**, 3827–3847.
50 S. J. Klatte and T. L. Beck, *J. Phys. Chem.*, 1995, **99**, 16024–16032.

51 (*a*) E. Manias, H. Chen, R. Krishnamoorti, J. Genzer, E. J. Kramer and E. P. Giannelis, *Macromolecules*, 2000, **33**, 7955–7966; (*b*) V. Kuppa, S. Menakanit, R. Krishnamoorti and E. Manias, *J. Polym. Sci., Part B: Polym. Phys.*, 2003, **41**, 3285–3298.
52 (*a*) A. Gaudel-Siri, P. Brocorens, D. Siri, F. Gardebien, J. L. Bredas and R. Lazzaroni, *Langmuir*, 2003, **19**, 8287–8291; (*b*) F. Gardebien, J. L. Bredas and R. Lazzaroni, *J. Phys. Chem. B*, 2005, **109**, 12287–12296.
53 D. R. Paul, Q. H. Zeng, A. B. Yu and G. Q. Lu, *J. Colloid Interface Sci.*, 2005, **292**, 462–468.
54 F. R. Jones, in *Interfacial Phenomena in Composite Materials*, ed. F. R. Jones, Buttersworths, London, 1989, p. 25.
55 J. Móczó and B. Pukánszky, *J. Ind. Eng. Chem.*, 2008, **14**, 535–563.
56 A. A. Gusev, *Macromolecules*, 2001, **34**, 3081–3093.
57 S. Bocchini, S. Morlat-Therias, J. L. Gardette and G. Camino, *Eur. Polym. J.*, 2008, **44**, 3473–3481.
58 C. Marega, V. Causin, A. Marigo, G. Ferrara and H. Tonnaer, *J. Nanosci. Nanotechnol.*, 2009, **9**, 2704–2714.
59 T. D. Fornes, P. J. Yoon, D. L. Hunter, H. Keskkula and D. R. Paul, *Polymer*, 2002, **43**, 5915–5933.
60 E. Bilotti, H. R. Fischer and T. Peijs, *J. Appl. Polym. Sci.*, 2008, **107**, 1116–1123.
61 S. Bocchini, S. Morlat-Therias, J. L. Gardette and G. Camino, *Polym. Degrad. Stab.*, 2007, **92**, 1847–1856.